Case Studies in Construction Materials 19 (2023) e02582

Contents lists available at ScienceDirect

Case Studies in Construction Materials

journal homepage: www.elsevier.com/locate/cscm

Case study

Lessons learnt from thermo-mechanical feasibility assessment of pavement solar collectors using a FE-ANN approach

Taher Ghalandari [a,*], David Hernando [a], Navid Hasheminejad [a], Mahesh Moenielal [b], Cedric Vuye [a]

[a] SuPAR Research Group, Faculty of Applied Engineering, University of Antwerp, Antwerp, Belgium
[b] TNO, Delft, the Netherlands

ARTICLE INFO

Keywords:
Energy harvesting
Pavement Solar Collector (PSC)
Asphalt pavement
Interface shear failure
Artificial Neural Network
Finite element method

ABSTRACT

This study presents a feasibility assessment of harvesting heat from asphalt pavement and a structural performance evaluation of a Pavement Solar Collector (PSC) in Utrecht, The Netherlands. The potential for interface failure was evaluated through experimental tests to determine the yield shear stress/strength ratio (YR) parameter. Subsequently, pavement responses were computed for two scenarios (with and without PSC) to evaluate damage factors using a bottom-up fatigue cracking approach. This study introduces a hybrid approach, combining Finite Element (FE) analysis with Artificial Neural Networks (ANN) to significantly reduce the computational time required for thermal FE simulations. This FE-ANN prediction model is employed to conduct parametric studies on three key input parameters of PSC systems: pipe embedment depth, inlet supply temperature, and pipe section length. The structural response analysis showed that the YR remained below 0.25 for temperatures below 32.5 °C, peaking at 0.68 for 45 °C, indicating a minimal risk of interface shear failure. Cumulative damage factor calculations for the two scenarios showed that operating the PSC system between May and September could yield an 18% reduction in overall damage. It was also established that pipe section length exerted the most profound influence on the thermal responses of the PSC among the three selected parameters. The investigation revealed that a PSC system's total annual heat harvesting capacity could achieve a noteworthy 1.17 GJ/m^2, accompanied by an average outlet water temperature of 15 °C. Moreover, an increase in pipe section length from 50 to 300 m resulted in a significant decrease of up to 50% in the total annual heat harvest capacity of the PSC system while simultaneously causing the outlet temperature to rise to 30 °C.

1. Introduction

The last two decades have seen a growing trend toward energy harvesting technologies from asphalt pavements. Energy extraction using Pavement Solar Collector (PSC) systems is one of the highly promising technologies due to the extensive availability of asphalt pavement in roads, parking lots, airports, and bicycle paths. Asphalt pavements have a great potential to absorb solar radiation due to

Abbreviations: PSC, Pavement Solar Collector; PE, Polyethylene; AC, Asphalt Concrete; ISS, Interface Shear Strength; YR, Yield shear stress/strength Ratio; FE, Finite Element; ANN, Artificial Neural Network.

* Correspondence to: Groenenborgerlaan 171, 2020 Antwerp, Belgium.
E-mail address: taher.ghalandari@uantwerpen.be (T. Ghalandari).

https://doi.org/10.1016/j.cscm.2023.e02582
Received 7 September 2023; Received in revised form 11 October 2023; Accepted 15 October 2023
Available online 16 October 2023

their dark colour and consequently, reach high temperatures in the summertime [1].

PSCs (also called hydronic asphalt pavement) incorporate a system of pipes embedded in the asphalt pavement through which water or other liquid is circulated. Depending on their construction, PSCs aim to extract heat from the asphalt pavement in the summertime and/or to inject heat to provide a snow/ice-free road surface and prevent the formation of black ice on the surface in winter. As a result, PSC systems could improve road safety, reduce the need for de-icing chemicals, and provide an energy-efficient way to heat outdoor spaces [2]. Nevertheless, limiting the cost-benefit analysis solely to the potential energy gain results in an unfavourable outcome in the majority of case studies. Hence, incorporating the potential impact on the structural performance becomes imperative.

In terms of structural performance, the application of PSCs can reduce the temperature gradient through the depth of the pavement, thus increasing its service life. Recent studies claimed that pavement service life could be extended between 3 and 5 years by using PSC systems [3,4]. This is due to controlling the temperature profile of the asphalt pavement, which could reduce distresses, such as top-down cracking, rutting, and fatigue cracking [5]. Conversely, the placement of pipe networks in the asphalt pavement disturbs the uniformity of the system, which could result in lower compaction quality and stress concentrations around the pipes. Zhu et al. [6] investigated the mechanical response of PSC systems subjected to traffic and temperature changes using Finite Element (FE) modelling, and they concluded that stress concentrations are more likely to develop around the pipes, and the higher tensile stress becomes more prominent between adjacent pipes. The study findings also indicated that stress concentration could be diminished by increasing pipe spacing and pipe depth. Nevertheless, such adjustments are likely to lead to a decline in energy-harvesting capacity. Zhou et al. [7] studied the pipes' influence on the pavement's structural response by analysing three indexes; bottom tensile stress, surface deformation, and equivalent stress. The structural performance was assessed in three load conditions: vehicle static (mechanical), thermal, and coupling mechanical and thermal loads. The results showed that although maximum bottom tensile stress values for asphalt pavement with a PSC system were higher than a pavement without PSC for the mechanical load, introducing PSC dramatically reduces (more than four times) maximum bottom tensile stress for thermal and coupling loads. In terms of surface deformation and equivalent stress, the study concluded that the temperature load had a greater impact on the structural response than the static vehicle load [7]. Therefore, during the design phase, the structural performance of PSCs presents a challenge, as proper pipe placement is critical. To ensure that the potential risks of structural damage remain within an acceptable range for the road, the generated tensile stresses must remain minimal, and the interface shear strength shall exceed the shear stress. From this point of view, the pipe depth is a key design parameter to fulfil a balanced trade-off between harvesting maximum heat (pipes closer to the surface) and minimum risk of structural damage (pipes deeper in the asphalt layer). Despite the importance of the structural response of PSCs, there remains a paucity of evidence on the optimum pipe depth and impact of PSC systems on damage reduction as a result of reduced asphalt pavement temperature profile. The first part of this paper aims to address some of these research gaps by focusing on interface failure potential at the PSC and asphalt layer boundary and assessing the cumulative damage resulting from bottom-up fatigue cracking for a pavement with and without PSC.

Regarding thermal performance, several studies have estimated the energy harvesting efficiency (defined as the ratio between extracted heat over incident solar radiation) of PSCs to range from 20% to 30% [5,8–10], with certain research studies achieving 50% efficiency [11,12]. The energy harvesting capacity of large-scale PSCs is influenced not only by their geometrical properties and geographical location but also by operational conditions, as highlighted in a recent study [5]. Factors such as pipe spacing, flow rate, inlet supply temperature, and pipe embedment depth play a significant role in determining the efficiency of these systems [13]. Since a short time frame does not adequately represent the prevailing weather conditions that govern the system's performance throughout an entire month or season it is crucial to analyse its behaviour over an extended period rather than relying on a single day or even a week. However, the FE can be computationally expensive for long-term thermal simulations. To address this knowledge gap, this study adopted a machine learning strategy to propose a hybrid FE- Artificial Neural Network (ANN) approach to effectively minimise the computational time needed for simulations. The FE-ANN approach excels in providing rapid and accurate predictions of the long-term

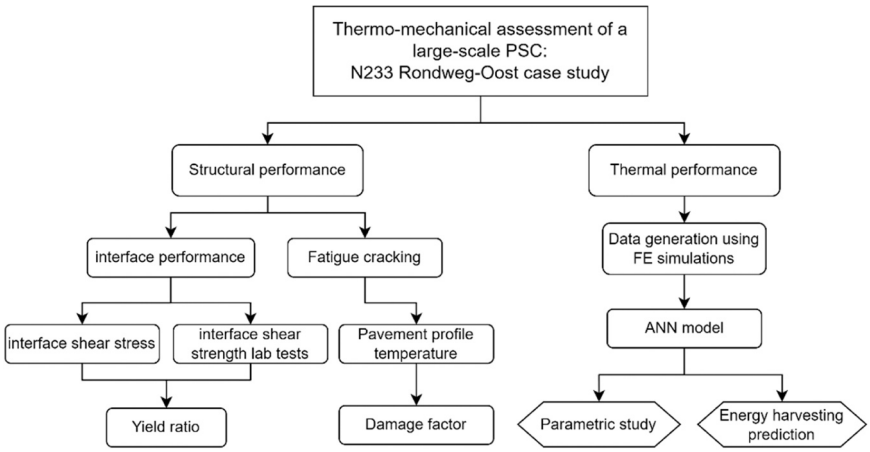

Fig. 1. Research methodology.

thermal performance of PSC systems, including heat harvest capacity and outlet water temperature.

This paper has been divided into seven sections, starting with this introduction. The second section provides the research methodology, followed by a description of the N233 Rondweg-Oost project in Section 3, which was used as a case study in this research. In section four, the structural performance of the PSC system with a focus on both interface shear strength and bottom-up fatigue cracking is investigated. The fifth section aims to predict PSCs' long-term energy harvesting capacity using a FE-ANN approach. That section begins by laying out the FE simulation framework and then describes the hybrid FE-ANN approach used in this study. The sixth section presents a parametric study focused on the three most influential PSC input parameters: pipe section length, pipe embedment depth, and inlet supply temperature. Finally, section seven provides a concise summary of the main conclusions of the study.

2. Research methodology

This study deals with both the structural and thermal performance of PSC systems, limited to asphalt pavements. Fig. 1 provides an overview of the research methodology used in this paper.

In the initial phase of structural response analysis, the assessment focuses on the potential for interface failure at the interface between the PSC system and the adjacent asphalt layer. The interface failure, commonly referred to as debonding, occurs when adjacent asphalt layers lose adhesion, leading to separation due to insufficient shear strength relative to the developed shear stress. This study employs a comprehensive approach, combining experimental and numerical methods, to evaluate the potential for interface shear failure. To calculate the stresses and strains in the pavement profile, a multilayer linear elastic analysis using KENPAVE software was adopted. Shear stresses were computed within the asphalt pavement profile under the tire edge at three distinct temperatures: 20 °C, 32.5 °C, and 45 °C, representing a range from intermediate to high temperatures. Subsequently, experimental tests were conducted to measure the Interface Shear Strength (ISS) of the asphalt interface under various conditions at the same temperatures. In assessing the potential for interface shear failure, this study employs the Yield Shear Stress/Strength Ratio (YR), which involves calculating the ratio of shear stress to interface shear strength at different temperatures.

The subsequent stage of the structural analysis was focused on examining how the activation of a PSC impacts the temperature variations within the asphalt pavement and subsequently influences damage accumulation. In this phase, we adopted the following bottom-up fatigue cracking calculation methodology. A validated FE simulation framework was employed to model the temperature gradient and profile across the asphalt pavement for two scenarios: with an integrated PSC system and a reference case without a PSC. Due to the cooling effect of the PSC, the profiles of pavement temperature differ, consequently affecting the stiffness of the asphalt material. As a result, these pavement temperature profiles were employed as inputs for estimating the stiffness of the asphalt layers. Subsequently, the Rubicon software that uses a multilayer linear elastic analysis approach was employed to compute the maximum tensile strain within the asphalt pavement for both aforementioned scenarios. Therefore, a damage factor is determined by applying Miner's incremental damage rule. A schematic flow chart for the structural performance analysis is shown in Fig. 2.

Thermal performance analysis of the PSC followed three main steps: generating data points using FE simulations, developing an ANN prediction model, and parametric study. In the first step, the validated FE model was utilised to simulate the thermal response of the PSC system over a period of six months, from the beginning of April until the end of September. In order to consider the average weather climate conditions, the average monthly weather data of the closest available weather station to the project between 2018 and 2021 were calculated. The data analysis revealed that 2020 closely approximated the four-year average. As a result, the Meteonorm* software was employed to collect the hourly weather data, which were then utilised for both thermal and structural simulations.

Due to the substantial influence of available data on the performance of ANN models, a set of simulations was conducted to generate data points, with a specific emphasis on the thermal response of PSCs concerning variations in pipe depth and inlet supply temperature. It is important to highlight that these simulations were limited to a minimum scope to mitigate the computational demands of FE models. This approach aligns with a key objective of this paper, which is to leverage ANNs to significantly reduce the computational time required for simulations. The subsequent phase involved the compilation of input weather data, PSC parameters, and outlet water temperatures derived from FE simulations into a database. This dataset was then utilised to train an ANN to construct a predictive model for the thermal performance of the PSC system. Ultimately, this developed ANN prediction model was employed to conduct a parametric analysis on pipe section length, pipe embedment depth, and inlet supply temperature to evaluate the response of heat harvesting capacity and outlet water temperature of the PSCs. The reader should bear in mind that although parameters such as pipe spacing and flow rate impact the efficiency of PSC systems significantly [13,14], due to practical constraints in the N233 Rondweg-Oost project, it is beyond the scope of this study to examine the response of PSCs on these factors.

3. N233 Rondweg-Oost (Veenendaal, The Netherlands) project description

This section provides an overview of the N233 Rondweg-Oost project, including the aim of the project, study plan, project location, vertical structure of the asphalt pavement and design load for structural analysis.

In collaboration with the municipality of Veenendaal, the Utrecht province (both in The Netherlands) has thoroughly investigated improving traffic flow, road safety, and accessibility along the N233 Rondweg-Oost in Veenendaal. In light of the insufficient management of the growing traffic volume and the planned expansion of the existing two-lane road to accommodate 2 × 2 lanes, a follow-

* meteonorm.com

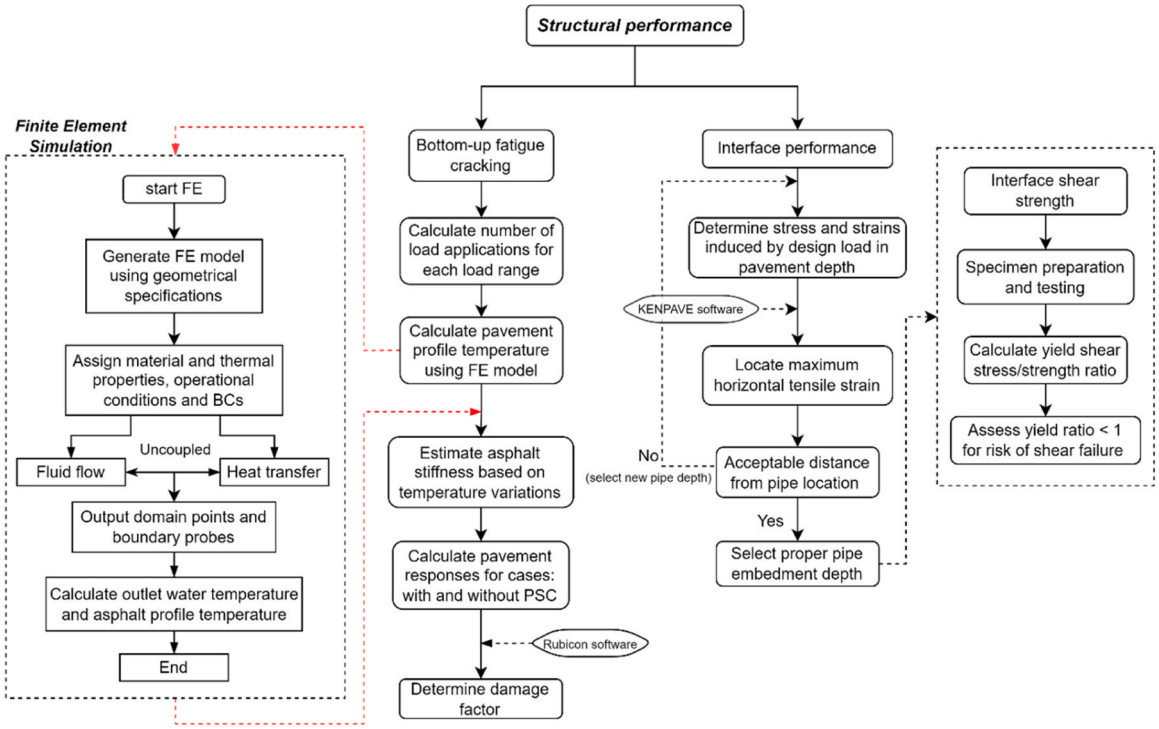

Fig. 2. Flowchart of the structural performance framework.

up study was proposed to investigate the potential of harvesting heat from the asphalt pavement and electricity from solar panels mounted on the noise barriers. The aim of this study phase was to assess the feasibility of generating heating and electricity from green and renewable sources for both residential and commercial buildings in the neighbourhood.

A weather station in De Bilt, Utrecht, the Netherlands, was selected as the closest station to the project site for the structural and thermal simulations. The locations of the De Bilt weather station and N233 Rondweg-Oost (Veenendaal) site location are shown in Fig. 3.

The structural composition of the asphalt pavement consists of a surface layer = 3 cm, binder layer = 4.5 cm, and base layer = 20 cm. The 27.5 cm of asphalt mixtures are placed on 30 cm of a hydraulic bound granular base layer. Details of the pavement structure, including thickness and asphalt types of the various layers, are presented in Fig. 4. The stiffness and Poisson's ratio of the granular layers are given in Table 1.

The stiffness of the asphalt mixtures depends on the temperature and the frequency of the applied load; thus, Eq. (1) was employed to calculate the stiffness of these materials [15].

$$\ln(E) = C_1 + C_2 \bullet T_{fict} + C_3 \bullet T_{fict}^2 + C_4 \bullet T_{fict}^3 \tag{1}$$

where E is the mixture stiffness (MPa), T_{fict} is the fictitious temperature (°C), and C_1, C_2, C_3, and C_4 are mixture-dependent coefficients. The values of these coefficients are provided in Table 1. Furthermore, a 50% reduction factor was used to estimate the stiffness of the low-noise surface layer (SMA – NL 8 G+) from that of a standard DL-C mix.

The fictitious temperature and equivalent traffic load frequency can be calculated as follows, see Eqs. (2) and (3) [15]:

$$\frac{1}{T_{fict}+273} = \frac{1}{T+273} - \frac{1}{11242}\log_{10}\left(\frac{8}{f_{eq}}\right) \tag{2}$$

$$\log\left(f_{eq}\right) = -0.6 - 0.5h_a + 0.94\log\left(V\right) \tag{3}$$

where T is the actual pavement temperature (°C), f_{eq} is equivalent traffic load frequency (Hz), h_a refers to asphalt layer thickness (m), and V is truck speed (km/h). For a speed of 80 km/h and a total asphalt concrete (AC) thickness of 27.5 cm, the estimated frequency is 11.3 Hz. Moreover, the design load used in the structural analysis was a 100-kN single axle with single tires and an inflation pressure of 800 kPa.

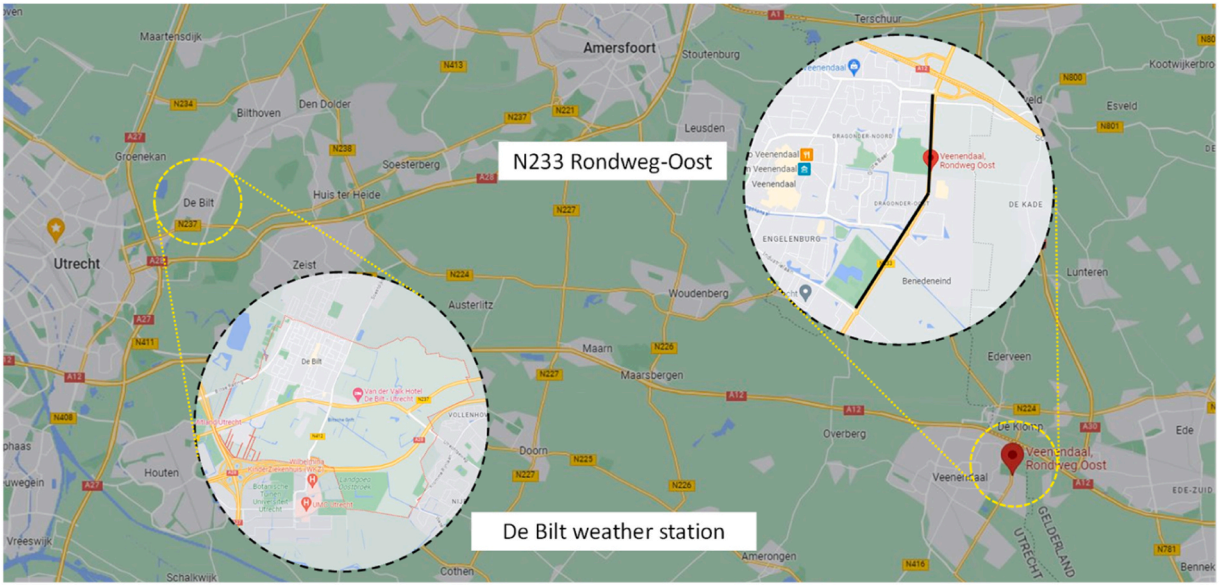

Fig. 3. N233 Veenendaal, Rondweg-Oost project location and weather station De Bilt.

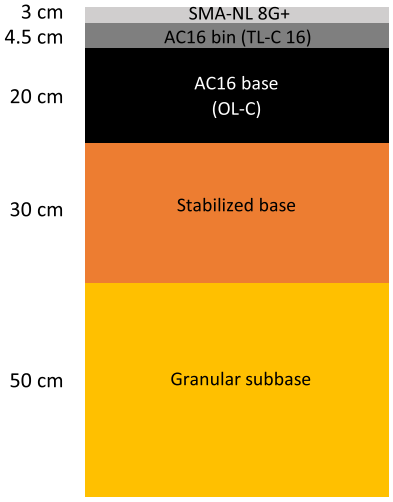

Fig. 4. Schematic structure of the designed pavement.

Table 1
Asphalt pavement structure and material properties [15].

Material	Thickness (cm)	Poisson's ratio (-)	Stiffness (MPa)	C_1	C_2	C_3	C_4
Surface	3	0.35	f(t)*	9.4198	-0.0184	-0.0011	0
Binder	4.5	0.35	f(t)*	9.4198	-0.0184	-0.0011	0
Asphalt base	20	0.35	f(t)*	9.6185	-0.0184	-0.0011	0
Stabilised base	30	0.35	600	-	-	-	-
Granular subbase	50	0.35	100	-	-	-	-
Subgrade	inf.	0.35	50	-	-	-	-

* The stiffness is a function of the asphalt temperature and frequency.

4. Structural performance: interface failure and fatigue cracking

In this section, the structural performance of the system was investigated. Firstly, a comprehensive structural analysis was performed to pinpoint the specific depths at which the implementation of the PSC could potentially lead to interface failure. The focus was not on slippage, caused by high longitudinal forces on the surface, but rather bending-induced failure of an interface deeper in the pavement structure [16,17]. Secondly, the impact of the introduction of the PSC on the asphalt pavement temperature profile, with an emphasis on traditional bottom-up fatigue cracking, was studied. By addressing both distress, this section provides valuable insights into the impact of integrating a PSC within an existing pavement infrastructure.

4.1. Assessment of interface failure potential

This section provides the analysis outcomes concerning the assessment of interface performance, and the comparison between shear stress and strength on the asphalt pavement. The computer software KENPAVE was employed to determine the stresses and strains induced by the design load through the depth of the pavement. The multilayer linear elastic analysis conducted with KENPAVE assumes all layers are continuous, homogeneous, isotropic, linear elastic, and fully bonded.

Fig. 5 illustrates the distribution of shear stress through the depth of the pavement under the tire edge at 20 °C, 32.5 °C, and 45 °C asphalt profile temperatures. The tire edge was chosen for analysis as it represents the location with the highest shear stress in the transverse direction [18]. Shear stress distribution indicates that the location of maximum shear stress changes, and the magnitude of stress also decreases with increasing temperature. At a cooler temperature of 20 °C, the maximum shear stress was observed at the bottom of the binder asphalt layer, approximately 7.5 cm below the surface. However, at a higher temperature of 45 °C, the maximum shear stress shifted to the bottom of the surface layer, located approximately 3 cm below the surface.

As previously stated, the shear strength of asphalt is strongly influenced by its temperature. To address this concern, a set of experimental tests was designed and conducted to measure the ISS of the asphalt interface under different conditions. Samples were cored with a diameter of 150 mm at multiple locations from asphalt slabs with a dimension of 60 cm × 40 cm and a thickness of 10 cm, which were prepared in the laboratory according to EN 12697–33. These specimens were tested using a guillotine-type fixture to shear the interface at multiple temperatures using a standard displacement rate of 50 mm/min in accordance with EN 12697–48. In this study, two distinct types of interfaces were investigated. The first type involved bonding two dense-graded asphalt (AC10 mixture) layers using a polymer-modified tack coat (Fig. 6-a). In the second type, a plastic grid with polyethylene (PE) pipes running in the longitudinal direction was placed at the interface between the two asphalt layers (Fig. 6-b). The same tack coat was applied both below and above the grid to ensure proper adhesion.

The ISS values were measured for both interface types at 20 °C, 32.5 °C, and 45 °C (Fig. 7). As expected, the results revealed a significant decrease in ISS as the temperature increased. Furthermore, introducing the grid resulted in an approximate 50% reduction in the bond strength of the interface across all temperature levels.

The reduction in ISS observed in the presence of the grid can be attributed to the smooth surface of the plastic grid, which creates a weak shear plane. Despite utilising a tack coat to promote bonding between the grid and the underlying asphalt layer, the smooth surface of the grid introduces a weak point in the interface. It should be noted that not all PSC systems utilise grids for pipe placement. Therefore, when evaluating the findings, it is recommended considering the specific design features of the PSC system being assessed.

To evaluate the potential for interface shear failure, this study utilised the ratio of shear stress to interface shear strength, yield shear stress/strength ratio (YR). Based on this definition, a YR equal to one corresponds with a material in a state of failure, whereas a zero value indicates no risk of shear-induced failure.

Fig. 8 depicts the YR for the three evaluated temperatures: 20 °C, 32.5 °C, and 45 °C. It was observed that the YR for temperatures

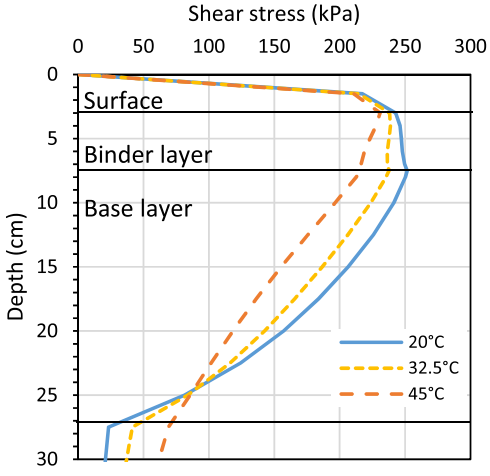

Fig. 5. Shear stress distribution through the depth of the pavement under the tire edge.

Fig. 6. Specimens after interface bond strength testing.

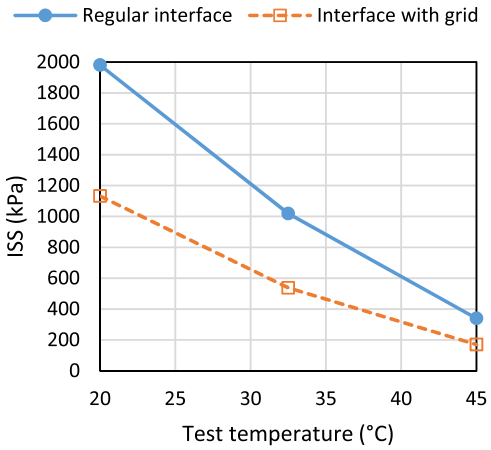

Fig. 7. Interface bond strength for different interface conditions and three temperatures.

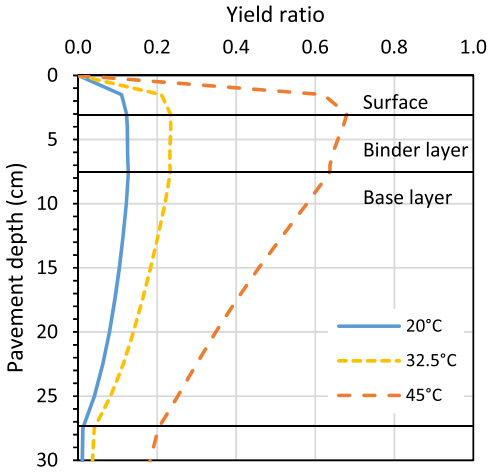

Fig. 8. The yield shear stress/strength ratio determined at three temperatures.

below 32.5 °C did not exceed 0.25, suggesting a minimal risk of shear failure. However, at the highest temperature of 45 °C, the YR reached its maximum value of 0.68 at the bottom of the surface layer. While the YR value remains below one, which indicates that shear failure slippage does not occur, the results suggest that the upper layers of the pavement are more vulnerable to interface shear failure.

In addition, the distribution of YR demonstrates a significant drop below the binder layer. Considering the YR distribution at high temperatures shown in Fig. 8, it is recommended placing the PSC system deeper than the binder asphalt layer. This placement will help minimise the risk of shear failure and ensure the pavement's structural integrity under elevated temperature conditions. According to the results in Fig. 8, at a temperature of 45 °C and a depth of 13.5 cm (which aligns with the bottom of a 6-cm-thick layer positioned below the binder layer), the YR is slightly below 0.5. This implies that the safety factor for shear failure in the pavement with a PSC placed 13.5 cm beneath the surface would be two at 45 °C. It should also be noted that if the pavement temperature at a depth of 13.5 cm does not reach 45 °C, potentially due to the cooling effect of the PSC during summertime, the safety factor against shear failure would be even higher.

4.2. Impact of PSC on bottom-up fatigue cracking

This section investigates the potential advantages of implementing a PSC due to the mitigation of extreme pavement temperatures, particularly in relation to damage accumulation. This part focuses on traditional bottom-up fatigue cracking due to the availability of well-established prediction models in this field.

The asphalt pavement temperature profile was calculated using a validated 3D FE model developed in a previous study. The FE model was simulated for only two representative months: June was determined to represent the climatic conditions from June to August, and May was the representative month for both May and September. It should be noted that the PSC system was assumed inactive during the other months due to its low efficiency in energy harvesting. The design parameters of the FE model to calculate the asphalt pavement temperature profile are as follows: pipe section length 100 m, pipe embedment depth 10 cm (from the pavement surface to the top of the pipe), water flow rate 180 l/hour (turbulent flow), and supply input temperature 12 °C. For more details on the development and validation of the FE model, see [13]. The approach followed to investigate bottom-up fatigue cracking is summarised in Fig. 2.

The total number of load repetitions over the design period was calculated using Eq. (4) [15]:

$$n = V \bullet a \bullet W \bullet O \bullet F_v \bullet F_R \bullet F_{reliability} \tag{4}$$

where V is the number of trucks per day and direction, a is the number of axles per truck, W is the number of workdays within a year, O is the traffic growth factor, F_v is a traffic speed correction factor, F_R is a correction factor to account for the number of lanes, and $F_{reliability}$ is a correction factor to take reliability into account for the uncertainty in the source for traffic loading (estimation / Weigh-In-motion system, etc.). The specific values assigned to each factor are presented in Table 2. The reference load spectrum was utilised to determine the number of load applications for each load range, as demonstrated in Table 3.

The FE simulations were performed for a reference year (2020) using available climatic data to predict the hourly pavement temperature profile. Within the design period, it was assumed that all years had the same temperature distribution as the reference year. To form the gradient and profile temperature of the asphalt pavement, the hourly temperatures were calculated at four depths: 1.5 cm (middle of the surface layer), 5.25 cm (middle of the binder layer), 12.5 cm, and 22.5 cm. In accordance with the AASHTO Mechanistic-Empirical Pavement Design Guide, the recommended approach involved calculating five quintiles (10th, 30th, 50th, 70th, and 90th) based on the hourly temperature distribution for each depth and month [19].

The pavement temperature profiles were utilised as inputs to estimate the stiffness of the asphalt layers using Eq. (1). A multilayer linear elastic analysis was performed with the Rubicon software to calculate the maximum tensile strain for all temperature quintiles, months of the year, load ranges, and scenarios with and without PSC. These simulations were conducted assuming a single axle with single tires and an inflation pressure of 800 kPa.

Miner's incremental damage rule defines damage at a specific condition as the ratio between the number of applied loads and the allowable number of load repetitions for that condition. The allowable number of load repetitions is calculated using the fatigue distress model in Eq. (5) [15]:

Table 2
Traffic factors used in the calculation of the number of load applications.

Factor	Value
Trucks/day/direction	2500
Axles/truck	3.5
Workdays	270
Fr (# lanes)	0.95
Fv (speed)	1
Annual traffic growth (%)	3
Design period (yr)	30
$F_{reliability}$	1.75

Table 3
Calculation of the number of load applications per load range.

Load range (kN)	Load (kN)	%	Axles/year	Total axles
20–40	30	26.62	597,453	49,742,100
40–60	50	32.22	723,138	60,206,253
60–80	70	18.92	424,636	35,353,889
80–100	90	9.46	212,318	17,676,945
100–120	110	6.50	145,884	12,145,892
120–140	130	4.29	96,284	8016,289
140–160	150	1.64	36,808	3064,502
160–180	170	0.26	5835	485,836
180–200	190	0.06	1347	112,116
200–220	210	0.03	673	56,058

$$N_f = SF \bullet \exp\left[C_a + C_e \bullet \left(\ln \varepsilon_t + C_b \bullet (\ln E)^2 + C_c \bullet \ln E + C_d\right)^2\right] \quad (5)$$

where SF is a healing factor equal to 4, ε_t is the maximum horizontal tensile strain in the asphalt layers, E is the asphalt mixture stiffness, and C_a, C_b, C_c, C_d, and C_e are mixture-dependent coefficients. Considering that the maximum tensile strain was observed at the bottom of the asphalt base layer, the damage calculation was specifically focused on this layer using the coefficients provided in Table 4.

Fig. 9 displays the annual distribution of damage for the scenarios with and without PSC. It is important to note that each month includes all load applications for that specific month over the entire 30-year period. The results clearly indicate that activating the PSC from May to September had a favourable impact on damage accumulation. When considering the cumulative damage for all months, it was observed that the total damage for the scenario incorporating a PSC was 18% lower than that for the scenario without a PSC. In other words, there is a significant decrease in bottom-up fatigue cracking damage over the 30-year design period, assuming the structural integrity of the pavement structure remains intact.

5. Prediction model development for thermal response of PSCs

In this section, a hybrid FE-ANN approach is proposed to predict the long-term thermal performance of a PSC system and perform a systematic sensitivity analysis. The developed prediction model has a dramatically reduced simulation time with acceptable accuracy. The details of FE simulations, data generation, and ANN model are discussed in the next subsections.

5.1. FE simulation framework: model development

This study used a FE modelling framework that was validated with the experimental results of a PSC prototype and showed a good agreement between the measured and predicted temperatures, both for the outlet fluid and the asphalt pavement surface temperatures [13]. Further details of the FE models, including the boundary conditions, mesh, and study solvers, are provided in [13,20].

The input parameters of the FE models were categorised into four groups, including material and thermal properties, geometrical design parameters, operational parameters and weather data. The thermophysical properties of the materials used in the FE simulations were adapted from literature and previous research studies on the PSC prototype performed by the authors (Table 5).

The geometrical specifications include the structural composition of the asphalt pavement, pipe spacing (centre-to-centre distance), pipe embedment depth (pavement from surface to the top of the pipes), and pipe section length. The pipe network has a serpentine configuration within the heat exchange layer with a centre-to-centre pipe spacing (P_s) of 15 cm. The outer and inner diameters of the PE pipes are $D_{out} = 20$ mm and $D_{in} = 13$ mm, respectively. In the FE models, the geometry of the PSC was designed for one side of the road, with a combination of six connected heat exchange sections, each of them with 1.80 m x 4.25 m dimensions. The pipe length of each heat exchange section is 50 m resulting in a 300 m total length of embedded pipes for the developed FE models. The length and width of the PSC system are $W = 1.80$ m and $L = 25.50$ m, resulting in a total net area of 45.90 m^2. As a part of the operational parameters, the water flow rate was set to 3 litre/min (180 l/hour) with a continuous operation mode, meaning that the system was

Table 4
Coefficients for the calculation of the allowable number of load repetitions (AC Base OL-C mix type) [15].

Coefficient	Value
C_a	39.176
C_b	-0.0645
C_c	1.404
C_d	-1.058
C_e	-0.212

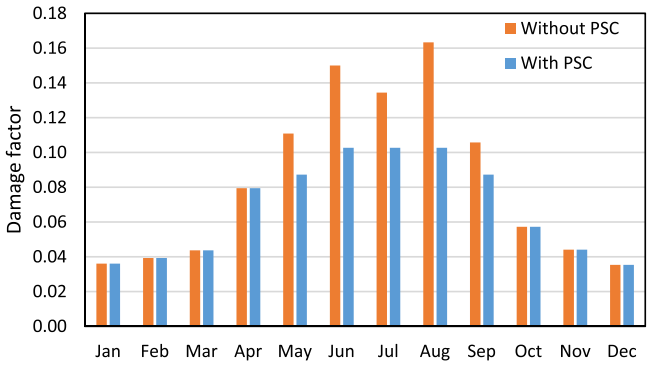

Fig. 9. Damage accumulation in terms of bottom-up fatigue cracking for scenarios with and without PSC.

Table 5
Material and thermal properties used in the simulations.

Material	Density (kg/m^3)	Thermal conductivity (W/m·K)	Heat capacity (J/kg·K)
Asphalt pavement	2340	1.5	1000
Compacted Aggregates	2000	0.575	1200
Soil	2200	0.75	1000
PE pipe	940	0.40	2300

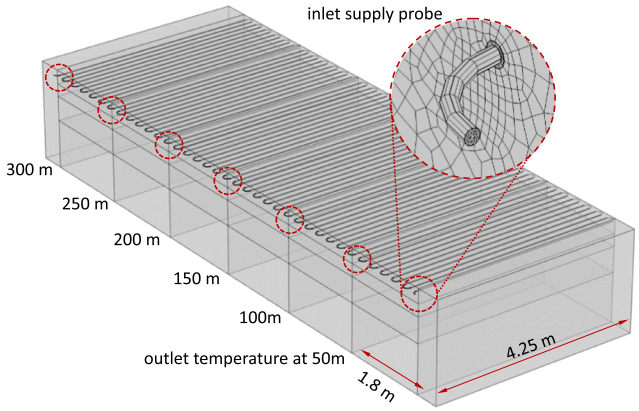

Fig. 10. Schematic of PSC system with inlet and outlet water probes at 50–300 m pipe section lengths.

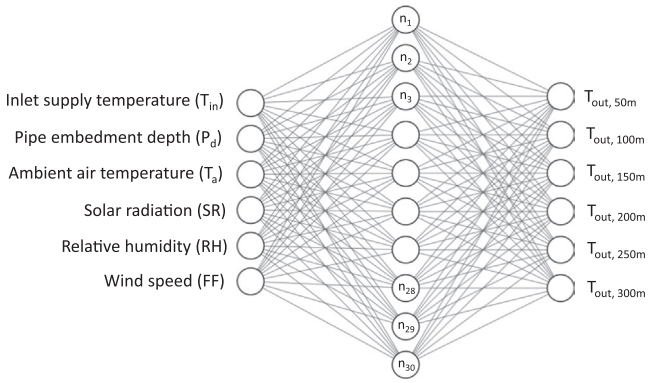

Fig. 11. The network structure of the ANN model.

operational 24/7 during the selected months. The FE model of the PSC system with inlet and outlet water temperature probes at various pipe section lengths is shown in Fig. 10.

5.2. ANN model

ANNs have found widespread applications in road engineering due to their ability to model complex relationships and make accurate predictions [21,22]. The various applications of ANNs to predict the performance of solar energy collectors have been extensively studied in [23], where they indicated that the utilisation of ANN techniques proves to be highly suitable for accurately predicting the performance of such systems with less calculation time than any other computational techniques. Although several studies have been carried out on predicting the performance of solar collectors using ANNs [24,25], only Masoumi et al. [26] have implemented ANNs to investigate PSC's performance. Therefore, in order to bridge this gap in the research, a new approach is proposed to simulate and predict the long-term thermal energy output (i.e., energy extraction capacity) of large-scale PSC systems.

A 3D FE analysis was conducted to investigate the impact of three variables: pipe depth, inlet supply temperature, and pipe section length over a six-month period in 2020. Through these simulations, a total of 11,500 data points were generated, representing input values for FE simulations and corresponding outlet water temperatures. Building upon these data sets, an optimised ANN model was developed to predict the thermal performance of the PSC system. The ANN algorithm was applied to the input data, including weather parameters, inlet supply temperature, and pipe embedment depth, to predict the outlet water temperatures at various pipe section lengths (Fig. 11). The weather data parameters are ambient air temperature (T_a), relative humidity (RH), wind speed (FF), and solar radiation (SR). The collected data were split into training, validation, and test sets with a 0.7, 0.15, and 0.15 ratio, respectively. The implemented approach involved utilising a feedforward neural network structure along with the Levenberg-Marquardt learning algorithm. In this study, the ANN has one hidden layer between input and output data with the tansig activation function and 30 nodes. The output layer has six nodes, equal to the number of probes at pipe section lengths in the PSC system to measure outlet water temperature (Fig. 10). The construction of the ANN model was accomplished using the MATLAB neural network toolbox. The network structure of the implemented 6–30–6 ANNs model is presented in Fig. 11.

6. A parametric study using ANN

In this section, a parametric study was carried out on three parameters: pipe section length [50–300 m], pipe embedment depth [75–150 mm], and inlet supply temperature [8–20 °C]. These parameters were selected based on a recent study that indicated that the heat harvesting capacity showed a high sensitivity to pipe spacing, flow rate, and inlet supply temperature, while pipe embedment depth and diameter have a marginal sensitivity response [13]. However, due to the origin of the current case study, parameters such as pipe spacing and flow rate were fixed for practical reasons, and their influence will not be investigated in further sections.

6.1. Influence of pipe section length on thermal outputs

This section investigates the thermal response of the PSC systems including heat harvesting capacity and outlet water temperature in various months with a focus on pipe section length. In the calculation of the heat harvesting capacity, first, the thermal performance simulations have been performed using both FE and ANN approaches for April to September 2020. Then, the yearly and monthly (for active 6 months) cumulative heat harvesting capacity have been calculated. The harvested heat q (kWh) from the PSC system was calculated using to Eq. (6) [13,20]:

$$q = \dot{m} \quad c_{p,w}(T_{out} - T_{in}) \tag{6}$$

where $\dot{m}$ (kg/s) is the mass flow rate, $c_{p,w}$ (J/kgK) is the specific heat capacity of water, and T_{out} (K) and T_{in} (K) are the outlet and inlet water temperatures in the PSC system.

To investigate the impact of the pipe section length on the thermal output of PSCs, four scenarios were defined as sub-problems derived from the introduced series configuration into the PSC system. These four different scenarios cover the same area of PSC with different pipe section lengths and are defined as follows:

Table 6
Heat harvesting capacity per unit area (kWh/m^2) of PSC for different pipe section lengths in April - September 2020 with (FR 180 l/hour, P_d 7.5 cm, and T_{in} 12 °C).

Pipe section length [m]	50		100		150		200		250		300	
	FE	ANN	FE	ANN	FE	ANN	FE	ANN	FE	ANN	FE	ANN
April	28.7	32.0	24.3	27.5	20.9	23.9	18.3	21.0	16.1	18.6	14.3	16.7
May	51.8	48.4	43.9	41.0	37.9	35.3	33.0	30.8	29.1	27.1	25.9	24.1
June	70.5	65.4	59.9	55.3	51.7	47.6	45.2	41.4	39.8	36.5	35.4	32.4
July	61.8	61.2	52.7	52.1	45.8	45.2	40.1	39.6	35.5	35.0	31.6	31.2
August	78.7	82.6	67.1	70.2	58.2	60.5	51.0	52.8	45.0	46.4	40.1	41.2
September	35.9	35.9	30.5	30.5	26.4	26.4	23.1	23.1	20.4	20.4	18.1	18.1
Total yearly	54.6	54.3	46.4	46.1	40.1	39.8	35.1	34.8	31.0	30.7	27.6	27.3

i. six (sections) x 50 m (pipe length each)
ii. three x 100 m
iii. two x 150 m
iv. one x 300 m

The long-term thermal performance calculations indicated that the PSC's total yearly heat harvesting capacity varies between 27.3 and 54.3 kWh/m^2 for 50–300 m pipe section length configurations. The heat harvesting capacity of PSC between April and September shows very similar results for FE and ANN approaches (Table 6). The difference between FE and ANN for the total yearly heat harvest is less than 2% in all four pipe length scenarios, demonstrating that the ANN algorithms are able to predict the outlet temperature of the PSC systems with a high degree of accuracy compared to FE models.

Furthermore, the pipe section length variation response on the harvested heat energy capacity shows that an increase in pipe section length decreases the heat gain in the PSC system. For example, an increase in pipe section length from 50 to 100, 150, and 300 m results in a 14.5%, 26.5%, and 49.5% decrease in total yearly heat harvest capacity. As a result, the pipe section length greatly impacts the heat harvesting capacity of the PSC and should be considered carefully in the design stage. The total yearly heat energy harvest in different pipe section length scenarios (calculated according to Table 6) demonstrate that the 6 × 50 m scenario has the highest heat gain (1.17 GJ/m^2), and the 1 × 300 m configuration is the lowest case with only 0.59 GJ/m^2.

Although the outlet water temperature is categorised as ultra-low-temperature, it can be combined with a heat pump to increase the temperature and used for various applications such as domestic hot water and heating system of the nearby buildings. The outlet water temperature is even more prominent compared to the heat harvesting capacity and should be assessed as a crucial output of the PSC systems. A proper decision-making approach seems essential for deciding the required outlet water temperature (depending on the application) and pipe section length (practical construction situation).

In this study, useful water temperature (ΔT) was defined as the daily average temperature difference between the inlet and outlet between 12:00–21:00 to assess the magnitude of the outlet water temperature. The pipe section length has a direct relationship with the heat harvesting capacity and useful water temperature. Fig. 12 compares the outlet water temperature and ΔT using FE simulation and ANN prediction model simulation and average daily ΔT for different pipe section lengths in June 2020. The output results indicate that the outlet water temperature and ΔT rise with an increase in pipe section length. With a constant 12 °C inlet supply temperature, a 50 m pipe section length brings about 15 °C outlet temperature, while it increases dramatically to around 30 °C in a 300 m pipe length. In terms of ΔT, the slope of increase is lower, and it increases from around 5–14 °C as a result of pipe section length variation from 50 m to 300 m.

Fig. 13 demonstrates the variation of the daily average outlet water temperature for three pipe section lengths as well as a comparison between FE vs ANN outputs. The daily average outlet water temperature variation for a 300 m pipe section length indicates that the outlet water temperature reaches above 30 °C in 8 days, while it barely reaches 20 °C in the case of the shortest pipe section length (50 m). The analysis of the data histograms of outlet water temperature for different pipe section lengths shows that the average daily outlet water temperature is concentrated at 20–25 °C. The results indicate that the outlet water temperature dramatically changes with the pipe section length; for instance, the outlet water temperature is less than 20 °C over 93% of PSC's operational time for the pipe section length of 50 m. With the increase of pipe section length to 150 m, the outlet temperature range moves to the higher temperature regions (with around 45% in the 20–25 °C range). Finally, with a 300 m pipe section length, the daily average outlet water temperature is greater than 25 and 30 °C for over 26% and 60%, respectively.

6.2. Pipe embedment depth

The response of pipe embedment and pipe section length changes on the yearly harvested heat in June 2020 is shown in Fig. 14. The results show that increasing pipe embedment depth decreases the heat harvesting capacity in the PSC system. An increase in pipe embedment depth from 75 mm to 150 mm reduces the heat gain capacity by 16.1% for the 50 m pipe section length. It should be highlighted that the YR exhibited its maximum value of 0.68 at a depth of 3 cm below the asphalt surface, corresponding to the placement of pipes at a depth of 10 cm, as elaborated upon in section ↱4.1. Consequently, the chosen pipe placement strategy appears to be secure against potential interface failure. Moreover, with an increase in pipe section length from 50 to 100 m and 100–150, the monthly heat harvest (for pipe depth of 75 mm) drops by 16.6% and 15%, respectively. However, an increase in pipe section length from 150 to 300 m, three times longer increase in pipe section length than other scenarios, will result in a 29.4% drop in monthly energy harvest.

The impact of pipe embedment depth on the outlet water temperature and ΔT with pipe section length and pipe depth variations is presented in Fig. 15. As expected, an increase in pipe embedment depth lowers both water outlet temperature and ΔT. Although a 50 m pipe section length with the closest pipe depth to the surface harvests a maximum yearly heat of 0.24 GJ/m^2 (Fig. 14), the magnitude of the output water temperature and ΔT (16.9 °C and 4.9 °C) are lower than for those of 150 m (22.3 °C and 10.3 °C) and 300 m (25.4 °C and 13.4 °C) pipe section lengths. As a result, a decision-making process on design variables is necessary depending on the project priority, such as maximum heat harvest or useful water temperature.

6.3. Inlet supply temperature

This section investigates the influence of the inlet supply temperature on the harvested yearly heat energy. Several research studies showed that the average soil temperature in Flanders and the Netherlands is around 10–13 °C below a certain depth (20–50 m) and can

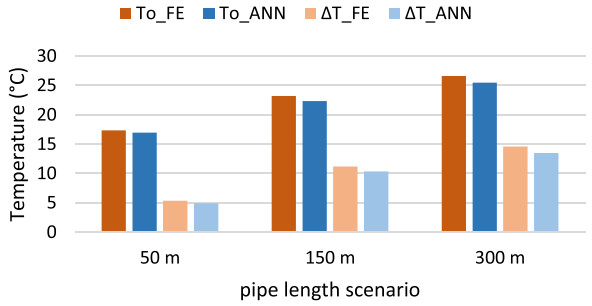

Fig. 12. The outlet and useful water temperature FE vs ANN for different pipe section lengths in June with (FR 180 l/hour, P_d 10 cm, and T_{in} 12 °C).

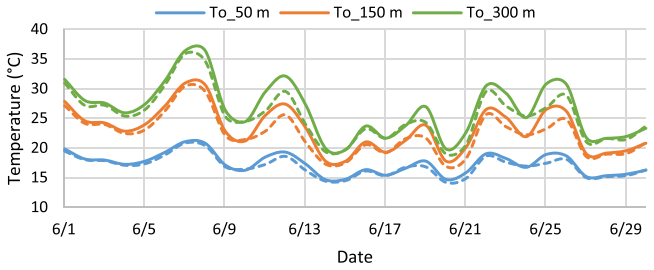

Fig. 13. The daily average outlet water temperature; FE (continuous lines) vs ANN (dashed lines) for different pipe section lengths in June with (FR 180 l/hour, P_d 10 cm, and T_{in} 12 °C).

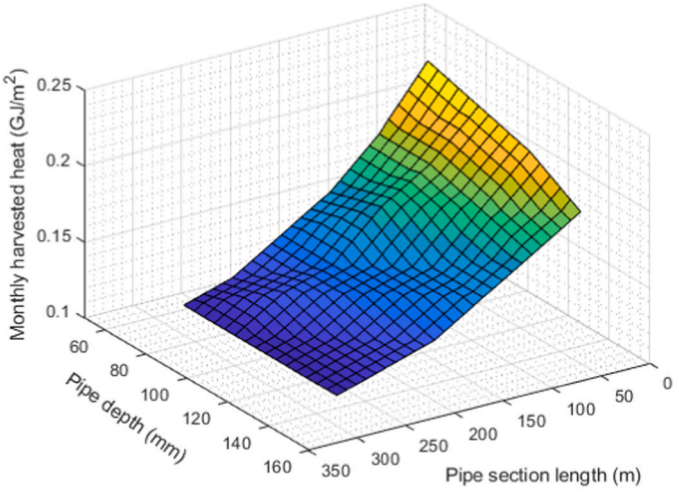

Fig. 14. Harvested monthly heat per unit area vs. pipe embedment depth and pipe section length for June 2020 with (FR 180 l/hour and T_{in} 12 °C).

be considered constant over the year [27,28]. In a recent study, the undisturbed ground temperature inside a borehole well at the University of Liege, Belgium, was measured at around 10 °C in February [27]. The groundwater temperature was measured around 12–13 °C in the Netherlands, considering that seasonal temperature variations can be higher if the source is close to a river and groundwater is influenced by riverbank filtration [28]. The current study uses the reference results from literature studies, where the average ground temperature for different months was assumed to be stable over the year. To assess the sensitivity of the inlet temperature, the inlet supply temperature was varied between 8 and 20 °C to take into account the lowest and highest possible temperature boundaries of horizontal and vertical ground heat exchangers [29,30].

Fig. 16 shows the monthly harvested heat concerning the variation of inlet supply temperature and pipe section length for June 2020. It indicates that a maximum monthly harvested heat of 0.31 GJ/m^2 can be achieved by lowering both pipe section length and inlet supply temperature. Moreover, the response of inlet supply temperature to heat harvest has a greater slope compared to the pipe section length, showing the higher sensitivity of this parameter. The output results demonstrate that increasing pipe length from 50 to 150 and 300 m results in approximately 25% and 48% drop in monthly heat harvest, independent from inlet supply temperature. With

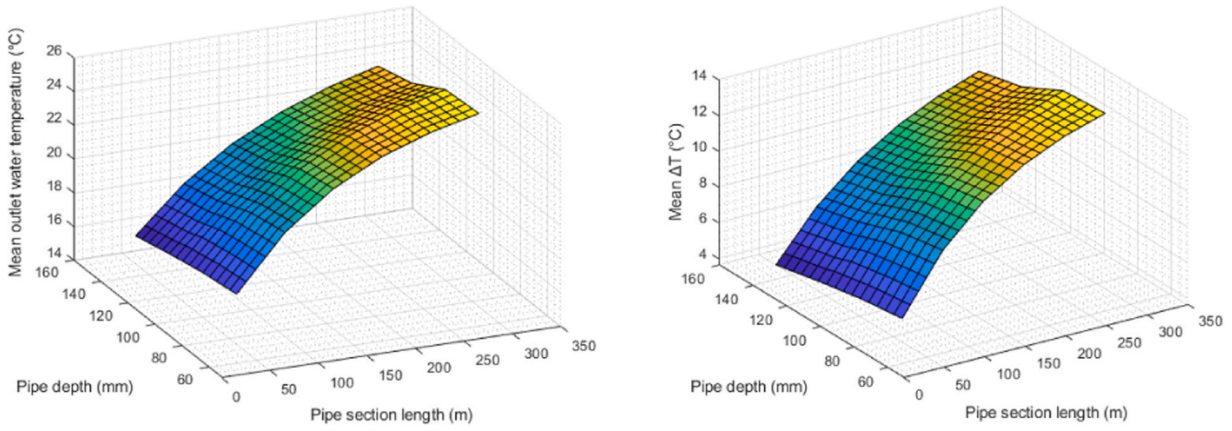

Fig. 15. Outlet water temperature (left) and ΔT (right) for pipe depth vs pipe section length for June 2020 with (FR 180 l/hour and T_{in} 12 °C).

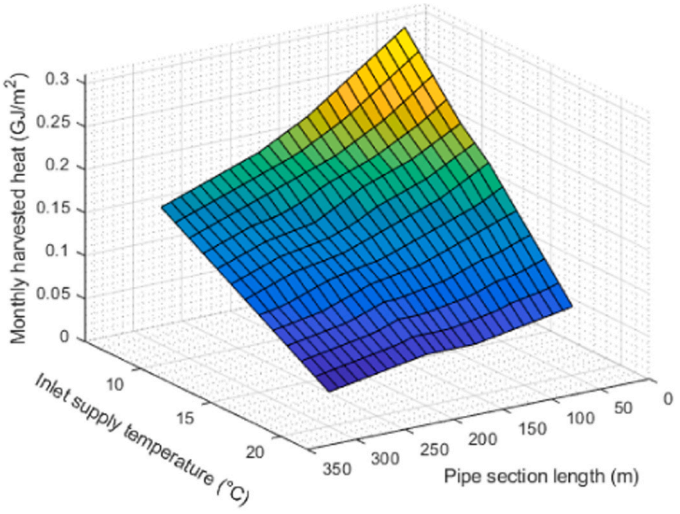

Fig. 16. Harvested monthly heat per unit area vs inlet supply temperature and pipe section length for June 2020 with (FR 180 l/hour and P_d 10 cm).

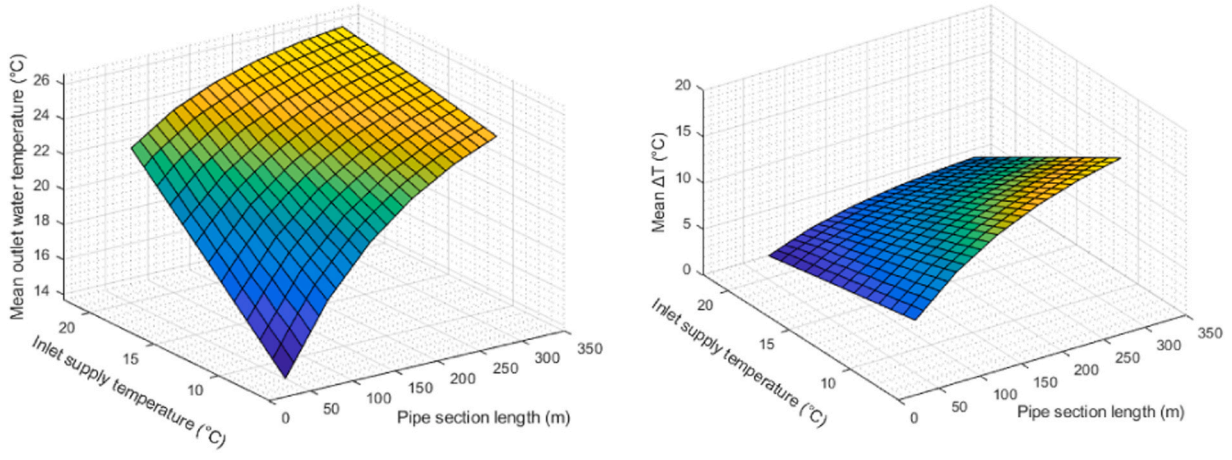

Fig. 17. Outlet water temperature (left) and ΔT (right) response for inlet supply temperature vs pipe section length with (FR 180 l/hour and pipe depth 10 cm).

respect to inlet supply temperature, increasing it from 8 °C to 12, 16, and 20 °C brings about a 25.8%, 48.3%, and 74.1% decline in monthly heat harvest (at 50 m pipe section length), respectively.

Fig. 17 demonstrates the variation of pipe section length and inlet supply temperature and their response to the outlet water temperature and ΔT, where an increase in pipe section length raises the outlet water temperature and mean ΔT. According to Fig. 17 – left, with an increase of pipe section length from 50 to 300 m, the outlet water temperature surges by 80.1%, 52.2%, and 18.1% for 8, 12, and 20 °C inlet supply temperatures. These outputs point out that the inlet temperature dramatically prevails over the pipe section length variation in lower inlet temperatures. The relative difference between 8 and 16 °C inlet supply temperatures for various pipe section lengths shows a more prominent impact of lower pipe section lengths. For instance, at 50 m pipe section length, the relative difference between 8 and 16 °C inlet is 43.2% compared to 5.3% for 300 m. Consequently, it can be deduced that as the length of the pipe section increases, the impact of the inlet temperature on the outlet temperature response becomes insignificant.

As discussed earlier in this section, the temperature magnitude of outlet water is as valuable as the amount of harvested heat from asphalt pavement. This is because the ultra-low-temperature outlet water should have a useful application prior to being combined with external sources. The longer pipe section lengths allow the fluid to travel a longer path in the pipes, resulting in an increased heat transfer between fluid, pipes, and asphalt. Hence, pipe section length increase positively influences both outlet water temperature and ΔT. In contrast, a longer pipe section length (with constant pipe spacing) has a greater PSC area that directly impacts the ratio of harvested heat per m^2 of the section. Therefore, although a shorter pipe section length in a PSC system brings higher heat harvesting capacity, the magnitude of the outlet and useful water temperature diminishes.

7. Conclusions

This study investigated the thermo-mechanical behaviour of Pavement Solar Collector (PSC) systems, restricted to asphalt pavements. In this paper, the structural response focused on assessing the cumulative bottom-up fatigue cracking damage and the potential of interface shear failure to address part of the research gaps in the literature. Moreover, a FE-ANN approach is developed to predict the long-term thermal performance of PSCs, including heat harvest capacity and outlet water temperature. The main findings are summarised as follows:

- It was observed that the yield shear stress/strength ratio (YR), defined as shear stress to the shear strength of an interface, reached 0.25 and 0.68 for profile temperatures of 32.5 °C and 45 °C at the bottom of the surface layer. These results prove that the upper layers of the pavement are more vulnerable to interface shear failure. In the binder layer at a depth of 13.5 cm, the YR was calculated around 0.5 for 45 °C, indicating a safety factor of two for shear failure in the pavement with a PSC placed at this depth.
- In terms of bottom-up fatigue cracking, it was proved that activating the PSC from May to September reduced the total damage over the design period by 18%.
- The developed hybrid FE-ANN model predicted the total yearly heat harvest within 2% error, demonstrating good accuracy of the model in predicting the outlet water temperature. Also, the model estimated that the PSC's total yearly heat harvesting capacity between 0.59 and 1.17 GJ/m^2 when the pipe section length ranged from 50 to 300 m.
- Through a systematic parametric study of three factors, the pipe section length showed the greatest impact on the thermal responses of the PSC. In terms of the heat harvesting capacity of the PSC, an increase in pipe section length (from 50 m to 300 m) decreased the total yearly heat harvest capacity of the PSC system by up to 50%. Conversely, the outlet water temperature and the useful water temperature (ΔT) demonstrated a positive correlation with pipe section length. Specifically, with an increase in pipe section length from 50 to 300 m, both the outlet temperature and ΔT escalated from 15° to 30°C and from 5 to 14 °C, respectively.
- The parametric study on pipe embedment depth showed that an increase in pipe embedment depth from 75 to 150 mm reduced the heat gain by 16.1% while an increase in pipe section length from 50 to 300 m, independent from pipe depth, resulted in around a 45–50% drop in monthly energy harvest.
- For the inlet supply temperature, an increase from 8 °C to 16 °C caused a 48% drop in monthly heat harvest, similar to that of a pipe section length increase from 50 to 300 m (independent from inlet supply temperature). Moreover, it was found that a maximum monthly harvested heat of 0.31 GJ/m^2 can be achieved with a 50 m pipe section length and 8 °C inlet supply temperature in a summer month. In terms of the outlet water temperature and ΔT, an increase in pipe section length raises these two values, whereas the inlet temperature dramatically prevails over the pipe section length variation in lower temperatures.

Based on the findings provided in this study, the following recommendations for future research can be made:

- Since the PSC system was continuously operational in the present study, the thermal performance of these systems in intermittent mode can be assessed and optimised.
- Further work should be conducted to evaluate the impact of the change in pavement temperatures induced by PSC systems on additional distress mechanisms like rutting or top-down cracking using more sophisticated distress models.

Declaration of Generative AI and AI-assisted technologies in the writing process

During the preparation of this work the authors used ChatGPT in order to improve the quality of the manuscript. After using this tool/service, the authors reviewed and edited the content as needed and take(s) full responsibility for the content of the publication.

Declaration of Competing Interest

The authors declare the following financial interests/personal relationships which may be considered as potential competing interests: Cedric Vuye reports financial support and administrative support were provided by Province of Utrecht.

Data Availability

The authors do not have permission to share data.

Acknowledgements

The first author also would like to acknowledge the University of Antwerp for the doctoral funding. The authors also would like to acknowledge the support of Utrecht province and Jeroen Daeij Ouwens during the initial phase of this research.

References

[1] J.L. Concha, J. Norambuena-Contreras, Thermophysical properties and heating performance of self-healing asphalt mixture with fibres and its application as a solar collector, Appl. Therm. Eng. 178 (2020), 115632.
[2] T. Ghalandari, N. Hasheminejad, W. Van den bergh, C. Vuye, A critical review on large-scale research prototypes and actual projects of hydronic asphalt pavement systems, Renew. Energy (2021).
[3] R.B. Mallick, B.-L. Chen, S. Bhowmick, Harvesting energy from asphalt pavements and reducing the heat island effect, Int. J. Sustain. Eng. 2 (3) (2009) 214–228.
[4] L. Dakessian, H. Harfoushian, D. Habib, G.R. Chehab, G. Saad, I. Srour, Finite element approach to assess the benefits of asphalt solar collectors, Transp. Res. Rec. 2575 (1) (2016) 79–91.
[5] T. Ghalandari, R. Baetens, I. Verhaert, D. Snm Nasir, W. Van den bergh, C. Vuye, Thermal performance of a controllable pavement solar collector prototype with configuration flexibility, Appl. Energy 313 (2022), 118908.
[6] X. Zhu, Q. Zhang, L. Chen, Z. Du, Mechanical response of hydronic asphalt pavement under temperature–vehicle coupled load: A finite element simulation and accelerated pavement testing study, Constr. Build. Mater. 272 (2021), 121884.
[7] B. Zhou, J. Pei, B. Richard Hughes, D. Snm Nasir, B. Vital, C.A.J. Pantua, J. Calautit, J. Zhang, Structural response analysis of road pavement solar collector (RPSC) with serpentine heat pipes under validated temperature field, Constr. Build. Mater. 268 (2021), 121110.
[8] H. Ceylan, K. Gopalakrishnan, S. Kim, W. Cord, Heated transportation infrastructure systems: existing and emerging technologies, in the 12th international symposium on concrete roads, Prague, Czech Republic (2014).
[9] J.W. Lund, Pavement snow melting, Geo-Heat. Cent. Q. Bull. 21 (2) (2000) 12–19.
[10] G. Guldentops, A.M. Nejad, C. Vuye, W. Van den bergh, N. Rahbar, Performance of a pavement solar energy collector: Model development and validation, Appl. Energy 163 (2016) 180–189.
[11] Z. Zhou, S. Hu, X. Zhang, J. Zuo, Characteristics and application of road absorbing solar energy, Front. Energy 7 (4) (2013) 525–534.
[12] J. Johnsson, B. Adl-Zarrabi, A numerical and experimental study of a pavement solar collector for the northern hemisphere, Appl. Energy 260 (2020), 114286.
[13] T. Ghalandari, A. Kia, D.M.G. Taborda, W. Van den bergh, C. Vuye, Thermal performance optimisation of pavement solar collectors using response surface methodology, Renew. Energy (2023).
[14] M. Pasetto, A. Baliello, A. Galgaro, E. Mogentale, A. Sandalo. Preliminary Study of an Energy Harvesting System for Road Pavements Made with Marginal Aggregate, Springer International Publishing, Cham, 2020. Proceedings of the 5th International Symposium on Asphalt Pavements & Environment (APE).
[15] CROW, *Ontwerpinstrumentarium asfaltverhardingen (OIA). CROW-rapport D11–05*. 2012.
[16] D. Hernando, J.A. Magruder, J. Zou, R. Roque. Localized Debonding as a Potential Mechanism for Near-Surface Cracking, 8th RILEM International Conference on Mechanisms of Cracking and Debonding in Pavements, Springer Netherlands, Dordrecht, 2016.
[17] B. Park, J. Zou, D. Hernando, R. Roque, J.A.M. Waisome, Investigating the use of equivalent elastic approach to identify the potential location of bending-induced interface debonding under a moving load, Mater. Struct. 54 (1) (2021) 18.
[18] D. Hernando, J.A.M. Waisome, J. Zou, R. Roque, Identification of potential location and extent of localized interface debonding in the wheelpath of asphalt pavements: Transp. Res. Rec. 2672 (40) (2018) 371–381.
[19] T. Officials, Mechanistic-empirical pavement design guide: a manual of practice, AASHTO (2020).
[20] T. Ghalandari, D. Ceulemans, N. Hasheminejad, G. Guldentops, W. Van den bergh, I. Verhaert, C. Vuye, A simplified model to assess the thermal performance of pavement solar collectors, Appl. Therm. Eng. 197 (2021), 117400.
[21] T. Ghalandari, L. Shi, F. Sadeghi-Khanegah, W.V. den bergh, C. Vuye, Utilizing artificial neural networks to predict the asphalt pavement profile temperature in western Europe, Case Stud, Constr. Mater. 18 (2023), e02130.
[22] N. Hasheminejad, G. Pipintakos, C. Vuye, T. De Kerf, T. Ghalandari, J. Blom, W. Van den bergh, Utilizing deep learning and advanced image processing techniques to investigate the microstructure of a waxy bitumen, Constr. Build. Mater. 313 (2021), 125481.
[23] H.K. Ghritlahre, R.K. Prasad, Application of ANN technique to predict the performance of solar collector systems - a review, Renew. Sustain. Energy Rev. 84 (2018) 75–88.
[24] F.J. Diez, L.M. Navas-Gracia, A. Martínez-Rodríguez, A. Correa-Guimaraes, L. Chico-Santamarta, Modelling of a flat-plate solar collector using artificial neural networks for different working fluid (water) flow rates, Sol. Energy 188 (2019) 1320–1331.
[25] M. Vakili, S.A. Salehi, A review of recent developments in the application of machine learning in solar thermal collector modelling, Environ. Sci. Pollut. Res. 30 (2) (2023) 2406–2439.
[26] A.P. Masoumi, E. Tajalli-Ardekani, A.A. Golneshan, Investigation on performance of an asphalt solar collector: CFD analysis, experimental validation and neural network modeling, Sol. Energy 207 (2020) 703–719.
[27] G. Radioti, K. Sartor, R. Charlier, P. Dewallef, F. Nguyen, Effect of undisturbed ground temperature on the design of closed-loop geothermal systems: A case study in a semi-urban environment, Appl. Energy 200 (2017) 89–105.
[28] C. Agudelo-Vera, S. Avvedimento, J. Boxall, E. Creaco, H. de Kater, A. Di Nardo, A. Djukic, I. Douterelo, K.E. Fish, P.L. Iglesias Rey, N. Jacimovic, H.E. Jacobs, Z. Kapelan, J. Martinez Solano, C. Montoya Pachongo, O. Piller, C. Quintiliani, J. Ručka, L. Tuhovčák, M. Blokker, Drinking Water Temperature around the Globe: Understanding, Policies, Challenges and Opportunities, Water 12 (2020), https://doi.org/10.3390/w12041049.
[29] G. Florides, S. Kalogirou, Ground heat exchangers—A review of systems, models and applications, Renew. Energy 32 (15) (2007) 2461–2478.
[30] H. Javadi, S.S. Mousavi Ajarostaghi, M.A. Rosen, M. Pourfallah, Performance of ground heat exchangers: A comprehensive review of recent advances, Energy 178 (2019) 207–233.